Monatshefte für Chemie - Chemical Monthly (2018) 149:2183–2193
https://doi.org/10.1007/s00706-018-2311-y

ORIGINAL PAPER

DFT study of double 1,3-dipolar cycloaddition of nitrilimines with allenoates

Mousa Soleymani[1]

Received: 31 July 2018 / Accepted: 1 October 2018 / Published online: 26 October 2018

Abstract

The double 1,3-dipolar cycloaddition reaction between nitrilimine and allenoate, experimentally investigated by Guo and co-workers, was theoretically studied at the B3LYP/6-311G** and wB97XD/6-311G** computational levels in both gas phase and dichloromethane solution. The results indicated that the formation of the experimentally reported product is clearly explained by the analysis of the calculated Fukui function reactivity indices as well as transition states studies. Frontier molecular orbitals analysis showed that the HOMO orbital of nitrilimine as donor is also the frontier effective-for-reaction molecular orbital (FERMO). Finally, on the basis of the Wiberg bond indexes and AIM analysis, it was found that all of the reactive channels proceed through an asynchronous concerted mechanism.

Graphical abstract

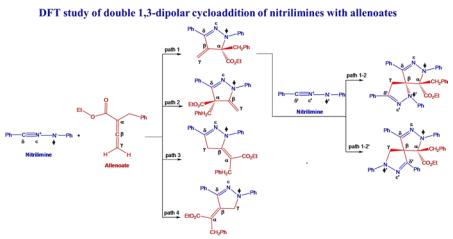

Keywords Cycloaddition · Nitrilimine · Transition state · Spirobidihydropyrazole · Charge transfer · FERMO

Introduction

In 1960, the general concept of the 1,3-dipolar cycloaddition was introduced by Huisgen [1]. This reaction involves interaction between two species, namely, 1,3-dipole and dipolarophile. While the 1,3-dipoles have four π electrons and are analogous with the allyl or propargyl anions, the dipolarophiles are typically substituted alkenes, alkynes, and allenes which may bond to certain functional groups such as carbonyl, imine, azo and nitroso. Due to the large variety of 1,3-dipoles as well as dipolarophiles, the 1,3-dipolar cycloaddition is a very excellent reaction for the synthesis of various five-membered heterocyclic rings. Also, owing to their high stereo- and regioselectivity, these cycloaddition reactions are useful in organic synthesis [2, 3].

Spiro compounds, or spiranes, are generally those compounds that present a twisted structure of two or more rings, in which the rings are connected together by one common atom [4]. Several categories of spiro compounds contain one or more certain heteroatoms such as oxygen, nitrogen and sulfur, which often occur naturally [5, 6]. Spiropyrazolines are a class of spiro heterocyclic compounds which have attracted significant interest in medicinal chemistry as they

Electronic supplementary material The online version of this article (https://doi.org/10.1007/s00706-018-2311-y) contains supplementary material, which is available to authorized users.

✉ Mousa Soleymani
m.soleymani@abru.ac.ir; m_soleymani2007@yahoo.com

[1] Department of Chemistry, Faculty of Science, University of Ayatollah Alozma Borujerdi, Borujerd 69199-69411, Iran

Scheme 1

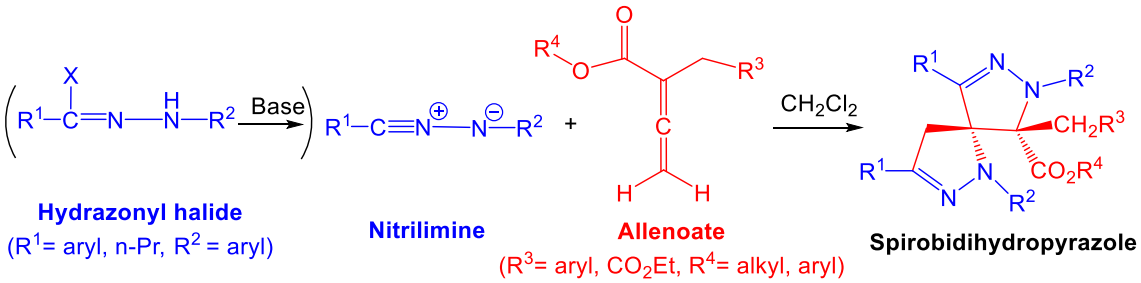

Scheme 2

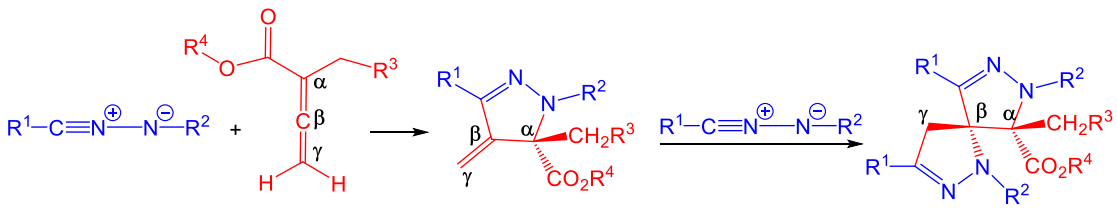

have pharmaceutical and biological properties such as antibacterial and anti-cancer activities [7–11].

In 2017, Guo et al. reported a double 1,3-dipolar cycloaddition reaction for the synthesis of spirobidihydropyrazole derivatives in which certain nitrilimines obtained in situ from the corresponding hydrazonyl halides were reacted with certain allenoates in dichloromethane (Scheme 1) [12].

The proposed mechanism is based on the interaction of nitrilimine with the C_α–C_β double bond of the allenoate at the first step to generate dihydropyrazoline intermediate. Then, the second molecule of nitrilimine performs the cycloaddition with the C_β–C_γ double bond of the dihydropyrazoline intermediate to produce the corresponding spirobidihydropyrazole (Scheme 2).

Since reliable theoretical calculations can confirm the experimental studies, we have investigated theoretically the 1,3-dipolar cycloaddition reactions of nitrilimine (**NI**) with allenoate (**Aln**) by DFT method in continuous of our previous theoretical studies on various organic compounds (Fig. 1) [13–16]. The important aims of the present work are:

- To elucidate the global and local reactivity indices of the reactants.
- A comparative study of the kinetic and thermodynamic aspects of the reaction.
- To elucidate the regioselectivity of the reaction.

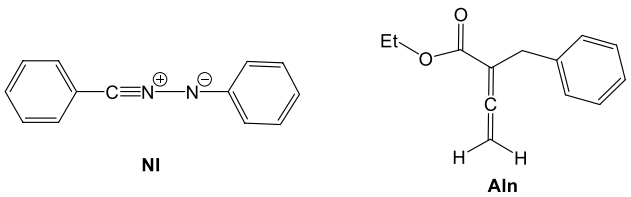

Fig. 1 The structure of nitrilimine (**NI**) and allenoate (**Aln**)

- Investigation of charge transfer at transition states.
- To study the bond formation and structural changes along the reaction coordinate.
- Determination and study of the reaction synchronicity.

Results and discussion

Determination of the most stable conformer of allenoate

To determine the most stable conformer of allenoate (**Aln**), the conformational analysis was performed and the molecular energies were calculated as a function of certain dihedral angles including C_β–C_α–C_{H2}–C_{Ph}, C_α–C_{H2}–C_{1Ph}–C_{2Ph}, C_β–C_α–C=O, C_α–C–O–C_{H2}, and C–O–C_{H2}–C_{H3} using wB97XD/6-311G** method. During the scan, the selected

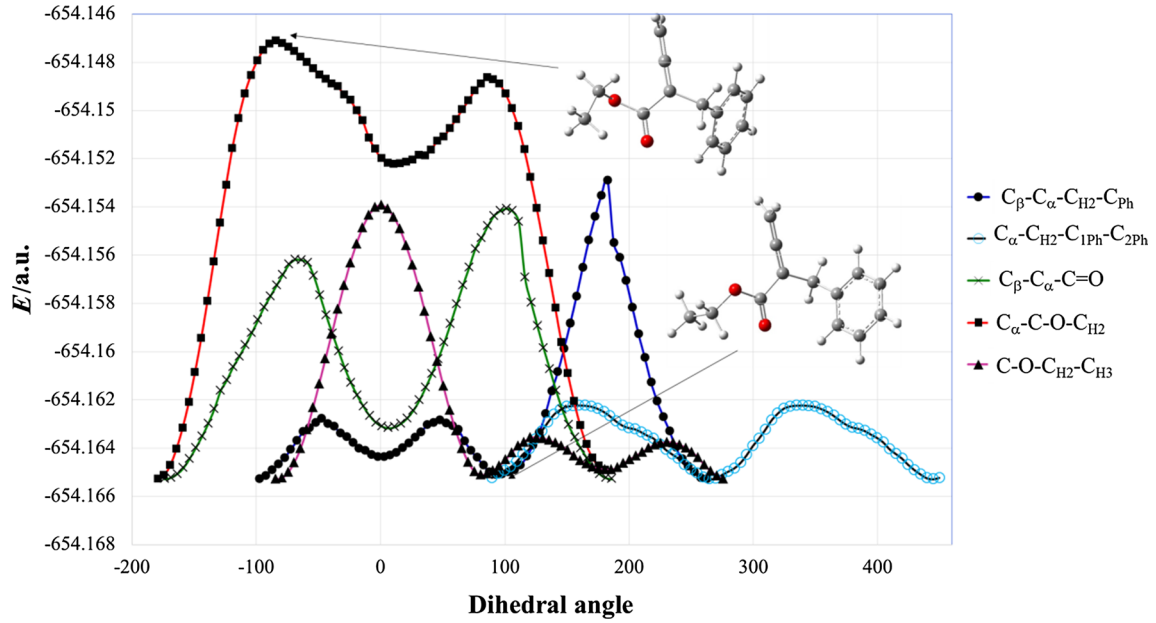

Fig. 2 The wB97XD/6-311G** calculated torsion potential for certain dihedral angles in compound **Aln** showing the geometries corresponding to the maximum and minimum energies

dihedral angle of **Aln** was increased by 5° in each step (Fig. 2). As seen in Fig. 2, several minima there are at the different torsional angles with molecular energy of − 654.1652 au. The corresponding geometries have the most stability, which probably can be attributed to the less electronic repulsion between the lone pairs on oxygen and π-electrons of the phenyl group. Alternatively, a global maximum is located around C_{α}–C–O–C_{H2} dihedral angle of − 84.4° with the molecular energy of − 654.1471 au. The corresponding geometry is the most unstable conformer which probably can be attributed to the staggered orientation of O–C_{H2} bond toward the C=O group. This orientation diminishes dramatically the hyper-conjugation effect between the bonding molecular orbital of O–C_{H2} bond (σ_{O-C}) and the anti-bonding molecular orbital of C=O group ($\pi^*_{C=O}$). According to the above results, the presented conformation at C_{β}–C_{α}–C_{H2}–C_{Ph} dihedral angle of 97.5° was selected for further calculations and studies (Fig. 2).

Analysis of the global DFT reactivity indices at the ground state of the reactants

Global DFT reactivity indices, namely chemical potential (μ), chemical hardness (η), and global nucleophilicity (N) are one of the useful tools for investigating the reactivity of the reactants as well as regioselectivity in the cycloaddition reactions [17]. Thus, to describe the reactivity and regioselectivity, the global DFT reactivity indices were calculated for **NI** and **Aln** in both gas and solution phases which is shown in Table 1.

Table 1 The B3LYP/6-311G** computed electronic chemical potential (μ), chemical hardness (η), and global nucleophilicity (N), for nitrilimine **NI** and allenoate **Aln** in the gas phase and solution (CH_2Cl_2)

Species	μ/eV	η/eV	N/eV
NI (gas)	− 3.46	1.76	4.15
Aln (gas)	−3.90	2.71	2.76
NI (CH_2Cl_2)	− 3.53	1.83	3.65
Aln (CH_2Cl_2)	− 3.97	2.75	2.20

The results presented in Table 1 indicate that the electronic chemical potential of **NI**, −3.46 eV in the gas phase and −3.53 eV in the solution, are relatively higher than those of **Aln**. Therefore, it can be concluded that along the corresponding reactions, the electron density is transferred from **NI** molecule toward **Aln** one. Also, the calculated values of the nucleophilicity index reveal that **NI** molecule is more nucleophilic than **Aln** one, and consequently, it can be deduced that the later acts as electrophile against the former.

Study of the regioselectivity of the reaction

To study the regioselectivity, four possible reactive channels were considered in which the reactants, **NI** and **Aln**, are added together to afford four regioisomeric adducts **I-P**, **II-P**, **III-P**, and **IV-P** (Scheme 3). As appears in reactive channels 1 and 2, the C_{α}–C_{β} double bond of **Aln** interacts with 1,3-dipole, **NI**, to generate two regioisomeric adducts **I-P** and **II-P**. Alternatively, two other regioisomers, **III-P**

Scheme 3

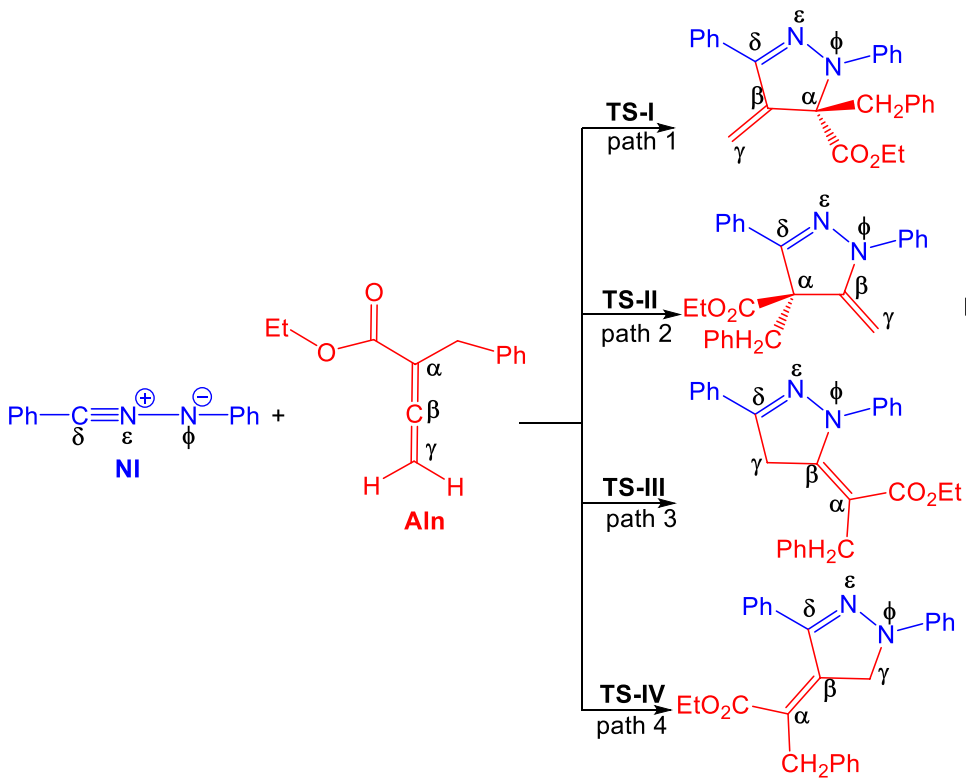

and **IV-P**, are generated when the C_β–C_γ bond of **Aln** undergoes cycloaddition reaction with **NI**. As mentioned in the introduction section, Guo et al. reported experimentally the regioselective formation of the **I-P** adduct in the first step of the cycloaddition reaction of **NI** with **Aln** [12].

In a polar reaction, when a non-symmetric nucleophile/electrophile pair react together, the most probable event is that the most nucleophilic center of nucleophile interacts with the most electrophilic center of electrophile. The Fukui functions are one of the most suitable tools to describe the reactivity of the reactants and regioselectivity of the products. In 1984, Yang and Mortier proposed an approach to the Fukui functions based on the variation of the Mulliken population of an atom, q_k, in a molecule [18]:

$$f_k^- = q_k(N) - q_k(N-1) \quad \text{for electrophilic attacks}$$

$$f_k^+ = q_k(N+1) - q_k(N) \quad \text{for nucleophilic attacks}$$

the local electrophilicity ω_k and local nucleophilicity N_k are respectively defined as:

$$\omega_k = \mathrm{w} f_k^+,$$

$$N_k = N f_k^-,$$

where ω and N are the global electrophilicity and nucleophilicity indices, respectively. The local parameters, ω_k and N_k, can be used satisfactorily to study the regioselectivity in various cycloaddition reactions.

To study the observed regioselectivity in the title reaction which is responsible of the formation of **I-P** adduct [12], the local electrophilicity and nucleophilicity indices were calculated from Mulliken population analysis. Since, in this reaction, **NI** and **Aln** act as nucleophile and electrophile, respectively, the local nucleophilicity (N_k) of **NI** and local electrophilicity (ω_k) of **Aln** were calculated and shown in Fig. S1 of Supplementary material.

A comparison of the results presented in Fig. S1 indicates that **NI** is more nucleophilically activated at the δ-carbon atom than the ϕ-nitrogen atom (the local nucleophilicity indices are $N_k = 0.628$ at the δ-carbon atom and $N_k = 0.528$ at the ϕ-nitrogen atom). On the other hand, **Aln** is more electrophilically activated at the β-carbon atom compared to the α- or γ-carbon atoms (the local electrophilicity indices ω_k are 0.040, 0.237, and 0.205 for α-, β-, and γ-carbon atoms, respectively). Therefore, the most nucleophilic and

Table 2 Relative enthalpies ΔH, entropies ΔS, Gibbs free energies ΔG, and the reactions rate constant k for the reactions of **NI** and **Aln** in the gas phase and dichloromethane calculated using B3LYP/6-311G** method

Species	ΔH/kJ mol^{-1}	ΔG/kJ mol^{-1}	ΔS/J mol^{-1} K^{-1}	k/s^{-1}
TS-I	46.74 (56.02)	105.81 (115.52)	− 197.70 (− 199.61)	1.78×10^{-6} (3.54×10^{-8})
I-P	− 207.15 (− 194.81)	− 132.84 (− 121.38)	− 248.59 (− 246.26)	–
TS-II	62.22 (70.04)	125.77 (133.39)	− 212.97 (− 212.46)	5.65×10^{-10} (2.62×10^{-11})
II-P	− 212.13 (− 199.41)	− 137.07 (− 126.98)	− 251.68 (− 243.02)	–
TS-III	85.60 (93.89)	148.87 (154.35)	− 211.53 (− 202.73)	5.07×10^{-14} (5.55×10^{-15})
III-P	− 233.13 (− 226.42)	− 159.37 (− 154.52)	− 247.09 (− 241.17)	–
TS-IV	64.06 (69.50)	120.79 (123.97)	− 189.95 (− 183.03)	4.22×10^{-9} (1.17×10^{-9})
IV-P	− 217.40 (− 212.00)	− 145.18 (− 132.88)	−241.81 (265.37)	–

The calculated parameters corresponding to the solution phase are given in parentheses

electrophilic centers are δ-carbon atom of **NI** and β-carbon atom of **Aln**. Accordingly, it should be expected that the most favorable nucleophile–electrophile interaction along the nucleophilic attack of **NI** on **Aln** will take place between the most nucleophilic center of **NI**, the δ-carbon atom, and the most electrophilic center of **Aln**, the β-carbon atom. This interaction can lead to the formation of either **I-P** (the experimentally reported adduct) or **IV-P** products.

Recently, Domingo reported the nucleophilic P_k^- and electrophilic P_k^+ Parr functions as an alternative and efficient tool for the study of the local reactivity in polar reactions [19, 20]. Parr functions are calculated based on the variations of spin electron-density that arise from electron transfer processes in polar reactions. Since, in the present study, compound **Aln** acts as electrophile (toward **NI**), the P_k^+ Parr functions of **Aln** and P_k^- of **NI** were calculated. Fig. S2 illustrates the obtained Parr functions of **NI** and **Aln** molecules.

Analysis of the results presented in Fig. S2 indicates that in contrast to the Fukui function, the Parr functions fail to predict the experimentally observed regioselectivity in the reaction. While similar to the Fukui functions, the electrophilic character of the β-carbon atom of **Aln** with P_k^+ of 0.422 is greater than the other allenic carbons, the nucleophilic character of the δ-carbon atom of **NI** with P_k^- of 0.182 is lower relative to the ϕ-nitrogen atom. Thus, the most favorable nucleophilic–electrophilic interaction is predicted to take place between C_β of **Aln** and N_ϕ of **NI**. This interaction can lead to the formation of either **II-P** or **III-P** regioisomeric adducts, which is in contrast to the experimental findings [12].

To test the aforementioned local reactivity indices and also to study the regioselectivity, the transition states associated with the reactions between nitrilimine **NI** and allenoate **Aln** were calculated. For this purpose, the reactive channels presented in Scheme 3 were simulated and their corresponding transition states were detected using B3LYP/6-311G** and wB97XD/6-311G** methods. Accordingly, the thermodynamic and kinetic parameters were calculated from optimized geometries of the reactants, transition states and products. Table 2 presents the B3LYP/6-311G** calculated thermodynamic and kinetic parameters in both gas and solution phases. The results obtained from wB97XD/6-311G** method are given in Table S3 of Supplementary material.

To achieve a better comparison between the results obtained for the all reactive channels, the corresponding free energies diagrams were drawn for both gas and solution phases which are shown in Fig. 3.

Analysis of the results presented in Table 2 and Fig. 3 indicate that:

(a) All four reactive channels are possible thermodynamically because the products corresponding to all reactive channels lie lower than the reactants. Although **III-P** is the thermodynamic product, but its corresponding transition state, **TS-III**, is energetically higher than the others.
(b) The path 1 and slightly path 4 are the most kinetically favorable reactive channels which is consistent with the results obtained from the Fukui reactivity indices. The reactive channel 1 leads to the formation of **I-P** adduct with a rate constant of 1.78×10^{-6} s^{-1} in gas phase which is approximately 400-fold higher than that obtained for the reactive channel 4. The reactive channel 1 is also approximately 35 million times faster than the reactive channel 3 (as mentioned above, the latter pathway leads to the formation of the thermodynamic product, **III-P**). Therefore, the regioselective formation of **I-P** adduct is in excellent agreement with the experimental outcomes [12].
(c) A similar trend is observed in the results of calculations in the gas phase with those in the solution.
(d) Generally, the polarity of the reactants, transition states and solvent can play an important role in the rate of the

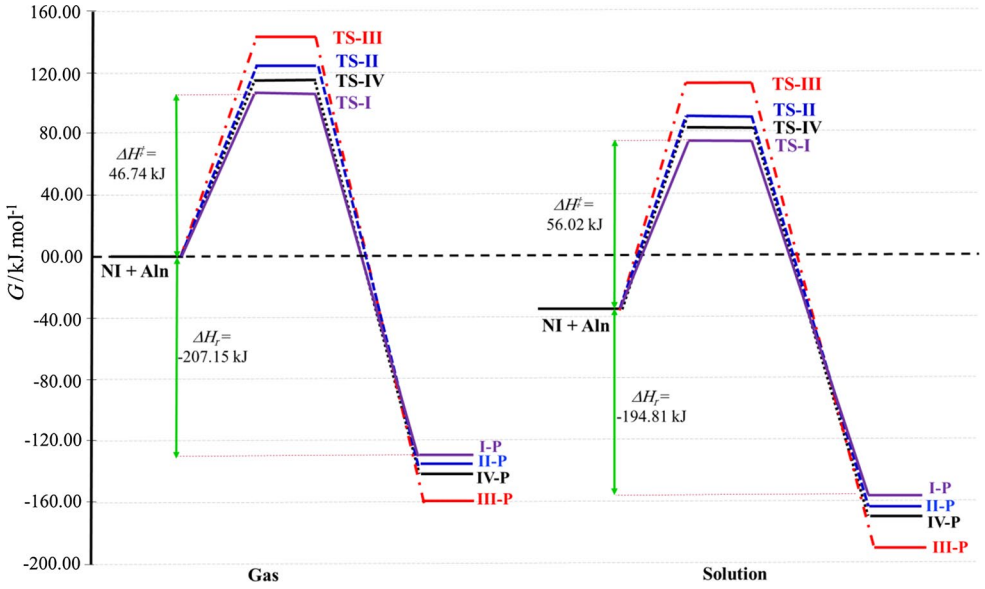

Fig. 3 The free energy diagram for the reaction of **NI** and **Aln** in the gas and solution phases

Scheme 4

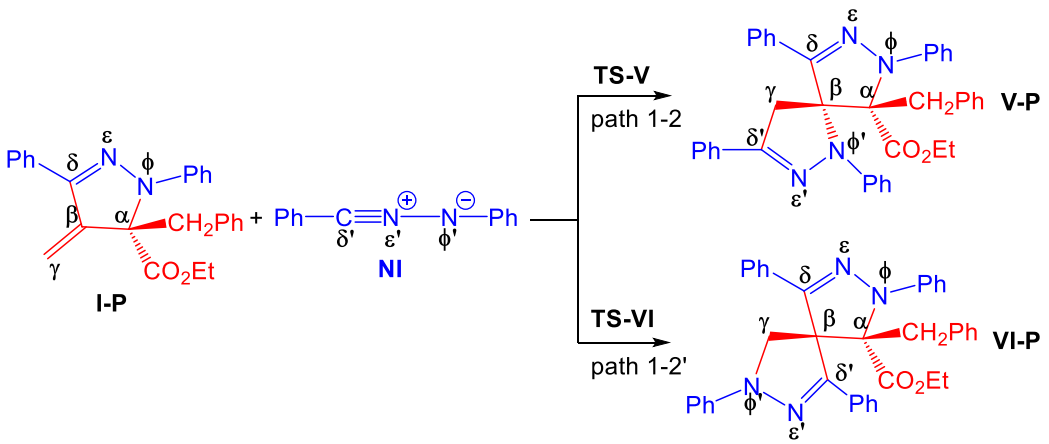

reactions. Since, the polarity of the reactants, especially **NI** as 1,3-dipole, is greater than that of the products, the rate of the reaction is reduced when the reaction is carried out in dichloromethane with dielectric constant of 8.93. Dichloromethane, as a low polar solvent, lowers the reactants energy level more than the transition states and increases the activation energy.

(e) The entropy of the reactions (ΔS) is reduced owing to the diminution of the freedom degrees of the reactants along the reaction coordinate.

Analysis of the data presented in Table S3 indicates that the results obtained from wB97XD/6-311G** method are in good agreement with those obtained from B3LYP/6-311G** method.

Since, the aforementioned theoretical results supported the experimental observations and predicted the formation of the **I-P** product, the second step of the reactive channel 1 was investigated in the next phase of the study. For this purpose, two possible reactive channels (1–2 and 1–2′) were considered between **I-P** and **NI** reagents. In these two reactive channels, the C_β–C_γ double bond of **I-P** reacts with **NI** in two different orientations, which leads to the generation of two regioisomeric adducts **V-P** and **VI-P** (Scheme 4).

As mentioned in the previous sections, the local reactivity indices obtained from Fukui functions described

Table 3 Relative enthalpies (ΔH), entropies (ΔS), Gibbs free energies (ΔG), and the reaction rate constant (k) for the reactions of **NI** and **I-P** in the gas phase and dichloromethane calculated using B3LYP/6-311G** method

Species	ΔH/kJ mol^{-1}	ΔG/kJ mol^{-1}	ΔS/J mol^{-1} K^{-1}	k/s^{-1}
TS-V	45.69 (50.79)	107.65 (113.89)	− 206.61 (− 210.92)	8.46×10^{-7} (6.83×10^{-8})
V-P	− 123.93 (120.21)	− 47.78 (48.07)	− 254.39 (− 241.29)	–
TS-VI	79.04 (88.78)	144.14 (152.84)	− 217.90 (− 214.89)	3.42×10^{-13} (1.02×10^{-14})
VI-P	− 115.77 (− 109.75)	−41.76 (− 34.94)	− 248.36 (− 249.45)	–

The calculated parameters corresponding to the solution phase are given in parentheses

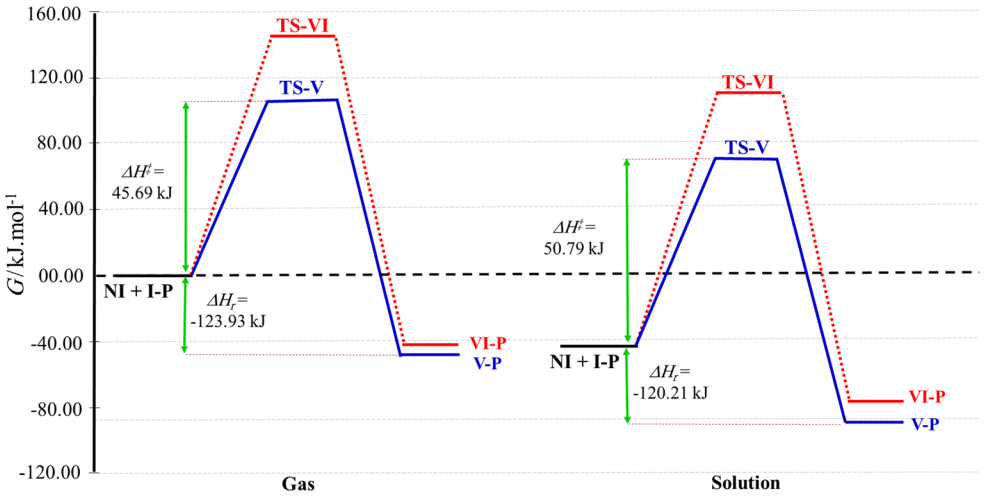

Fig. 4 Free energy diagram for the reaction between **NI** and **I-P** in the gas and solution phases

satisfactorily the observed reactivity and regioselectivity in the reactive channel 1. Therefore, the same indices were calculated for the reactive sites on **I-P** and **NI** reagents. The results are given in Fig. S3 of Supplementary material. The calculated electrophilic and nucleophilic Par functions of **I-P** and **NI** reagents are also presented in Fig. S3. Analysis of the local Fukui functions indicates that **I-P** is more electrophilically activated at the γ-carbon atom, $\omega_k = 0.328$, than the β-carbon one, $\omega_k = -0.004$ (which is slightly deactivated). Therefore, it is predicted that the most favorable nucleophile–electrophile interaction along the nucleophilic attack of **NI** on **I-P** will takes place between the most nucleophilic center of **NI**, the δ′-carbon atom, and the most electrophilic center of **I-P**, the γ-carbon atom. This event is in excellent agreement with the experimental outcomes, because the **V-P** adduct is the reported product for the title reaction [12]. Analysis of the calculated nucleophilic and electrophilic Parr functions designates the ϕ′-nitrogen atom as the most nucleophilic site ($P_k^- = 0.409$) of **NI** and the γ-carbon atom as the most electrophilic site ($P_k^+ = 0.274$) of **I-P**. These results suggest that a σ-bond should be formed between ϕ′-nitrogen atom of **NI** and γ-carbon atom of **I-P** which leads to the formation of unexpected **VI-P** adduct. Therefore, again the nucleophilic and electrophilic Parr functions fail to give a satisfactory description about the σ-bond formation between **NI** and **I-P**.

In the next step, to test the aforementioned local functions, the transition states corresponding to the two reactive channels between **NI** and **I-P** were detected using B3LYP/6-311G** and wB97XD/6-311G** methods in both gas and solution phases. Then, the thermodynamic and kinetic parameters were calculated from optimized geometries of the reactants, transition states, and products. The results are summarized in Table 3 and also in Table S4 of Supplementary material. Figure 4 depicts the free energy diagram for the reactions of **NI** and **I-P** in both gas and solution phases.

Analysis of the results presented in Tables 3 and S4 and Fig. 4 indicates that the reactive channel 1–2, which leads to the formation of **V-P** adduct, is more favorable both kinetically and thermodynamically. This reactive channel proceeds with a rate constant of 8.46×10^{-7} s^{-1} in gas phase which is approximately 250 thousand times faster than the reactive channel 1–2′. Thus, both local Fukui functions and transition states analysis predict the formation of **V-P** product, which is completely consistent with the experimental findings.

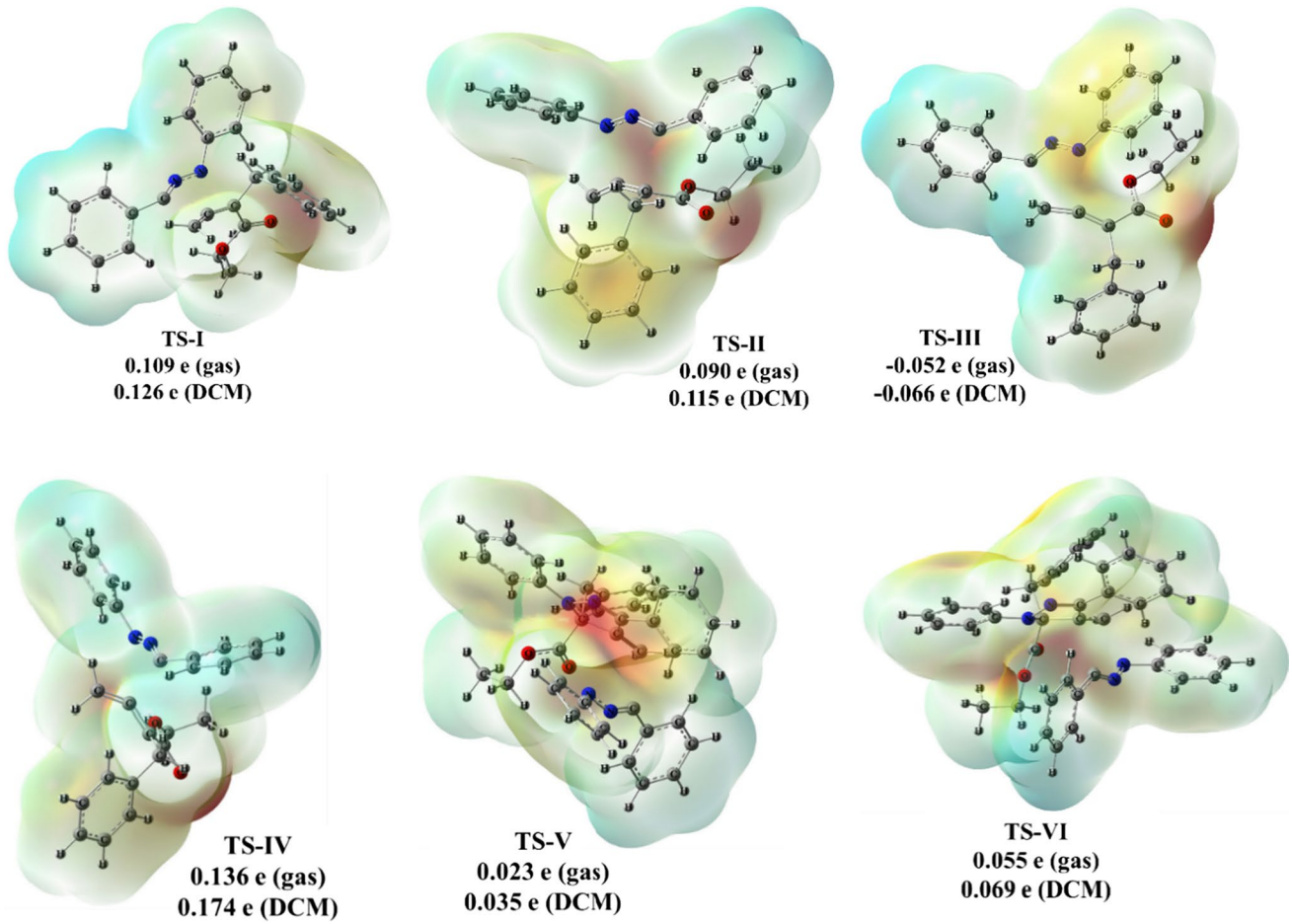

Fig. 5 The molecular electrostatic potential maps and the global electron density transfer (GEDT) values obtained for all transition states in both gas and solution phases. The red and blue colors represent the regions with high and low electron density, respectively (color figure online)

Study of charge transfer in transition states

The electrophilic/nucleophilic interactions are responsible of charge transfer processes in polar cycloaddition reactions. Global electron density transfer (GEDT) can be a relative criterion of charge transfer in transition states and sometimes determines the barrier energies [21]. Therefore, to study of charge transfer in the title reaction, the GEDT value was calculated for all transition states in both gas and solution phases. Figure 5 depicts the calculated values of GEDTs along with the molecular electrostatic potential map (MESP) of transition states. In the MESP map, the red regions are more negative, greater electron density, and the blue ones are more positive, lesser electron density.

Analysis of the GEDT values reveals that all transition states are relatively polar. In the case of **TS-I**, **TS-II**, and **TS-IV** transition states, the electron transfer takes place from **NI** fragment toward **Aln** one, while in **TS-III**, the most unstable transition state, the electron density is transferred from **Aln** fragment toward **NI** one. The yellow color in the molecular electrostatic map shows the regions with relatively high electron density which is observed for electron acceptor fragment. For both **TS-V** and **TS-VI** transition states it is noteworthy that the electron transfer takes place from **NI** fragment toward **I-P** one.

Interaction of the frontier molecular orbitals

How frontier orbitals are interacting? To answer this question, the energy differences between the frontier orbitals (HOMO/LUMO) of electron donor, **NI**, and electron acceptor, **Aln**, were calculated. The results indicated that the $HOMO_{NI}$–$LUMO_{Aln}$ energy difference, 4.03 eV, is less than that for $HOMO_{Aln}$–$LUMO_{NI}$ one, 4.92 eV. Accordingly, the interaction of the HOMO of **NI** with the LUMO of **Aln** is more favorable than the other alternative interaction. The results of the GEDT analysis confirmed also the $HOMO_{NI}$–$LUMO_{Aln}$ interaction. Recently, the frontier effective-for-reaction molecular orbital (FERMO) has emerged as a powerful approach to study the interaction of the frontier

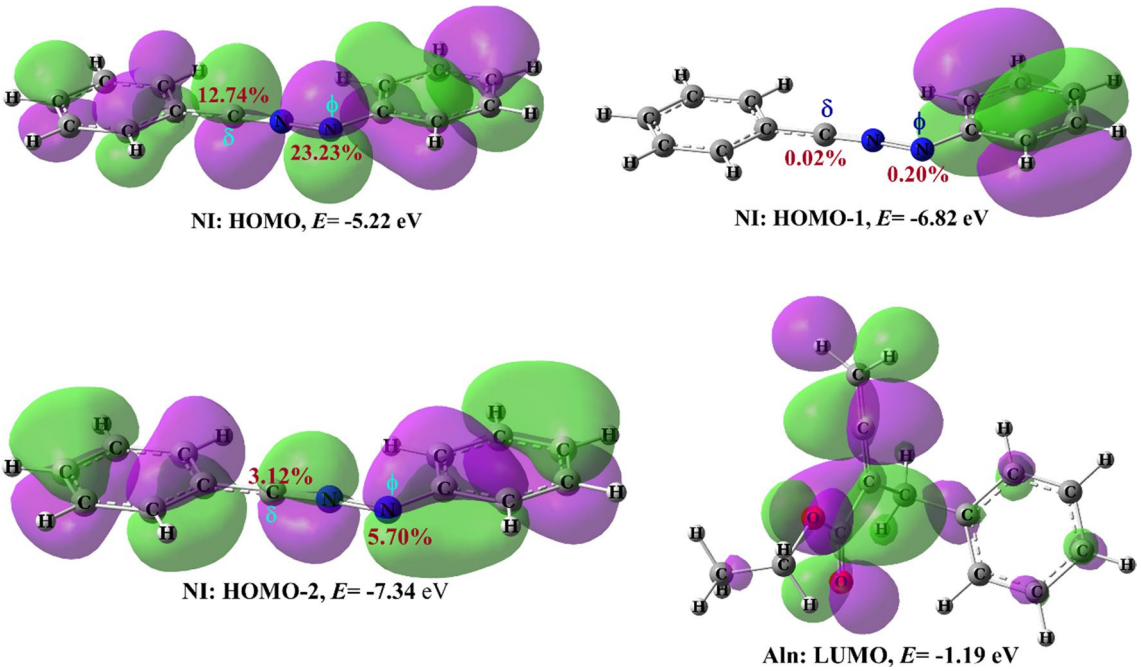

Fig. 6 The LUMO of **Aln** and the three highest occupied MOs of **NI** along with the relative contribution of the active sites

orbitals. This concept considers the HOMO or an occupied molecular orbital close to the HOMO with large contribution in atoms present at the active sites. For many reactions the FERMOs can work better than HOMO [22]. We used satisfactorily the FERMO concept to describe the reactivity of the active sites of the pyrene [13]. Therefore, to determine the frontier effective-for-reaction molecular orbital, we calculated the relative contribution of the active sites of **NI** (δ-carbon and ϕ-nitrogen atoms) in the three highest occupied MOs. The results are depicted in Fig. 6. On the basis of the composition and location of the molecular orbitals, it was found that the FERMO is the HOMO for the reaction, because the active sites of **NI**, the C_δ and N_ϕ atoms, have a larger contribution in the HOMO in comparison to the other occupied MOs.

Study of the synchronicity of the reactions

Since cycloaddition reactions are usually synchronous, the geometric features of the transition states were studied to understand the level of the synchronicity. Fig. S4 depicts the optimized structure of transition states along with their imaginary frequencies and the Wiberg bond indexes. Analysis of the Wiberg bond indexes reveals that the studied reactive channels are not completely synchronous, because the degree of advancement of the two new bonds between two fragments is not equal in the corresponding transition states. For example, in **TS-I** the bond index of C_β–C_δ, 0.282 in the gas phase, is more than that for C_α–N_ϕ, 0.125. Therefore, it can be said that the former bond is formed faster than the later. This trend is completely consistent with the results of the local Fukui functions, because the most favorable interaction was found to be a bond formation between C_β and C_δ atoms. A similar agreement is also observed for the reactive channel 1–2 between the Fukui function analysis and Wiberg bond indexes. Analysis of the bond indexes for the other transition states reveals that the considered reactive channels are not completely synchronous. Consequently, the bond index analysis indicates that these cycloaddition reactions take place via an asynchronous concerted mechanism.

AIM study of the cycloaddition reaction between NI and Aln

To understand the molecular mechanism of the cycloaddition reaction between **NI** and **Aln**, the AIM analysis was performed along the IRC profile associated with the most favorable transition state, **TS-I**, in the gas phase. In this method, the molecular topological graphs and the BCP electron densities (ρ) of the bonds that participate directly in the cycloaddition reaction, were calculated for some points located on the IRC path. The results are given in Fig. 7. At the first point associated with the IRC profile, P0, where the C_β–C_δ and C_α–N_ϕ distances are 3.0641 and 2.9760 Å, respectively, two interacting moieties, **NI** and **Aln**, are sufficiently far away from each other so that the corresponding BCP electron densities for C_β–C_δ and C_α–N_ϕ bonds are low ($\rho_1 = 0.01011$ and $\rho_4 = 0.01169$). As two reactants gradually

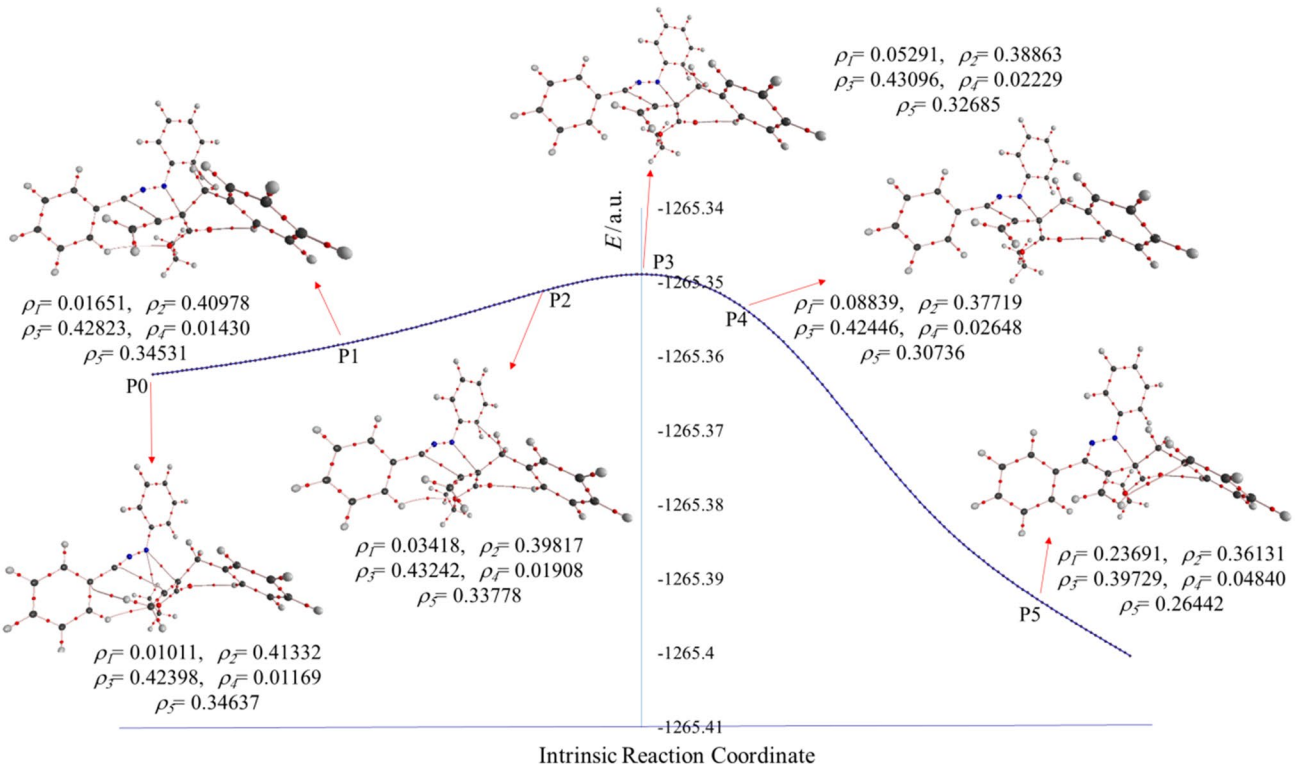

Fig. 7 B3LYP/6-311G** intrinsic reaction coordinate (IRC) profile of the most favorable transition state (**TS-I**) along with the BCP electron densities corresponding to C_β–C_δ (ρ_1), C_δ–N_ε (ρ_2), N_ε–N_ϕ (ρ_3), C_α–N_ϕ (ρ_4), and C_α–C_β (ρ_5) bonds for the cycloaddition reaction of **NI** with **Aln** in the gas phase

approach each other the BCP electron densities for C_β–C_δ and C_α–N_ϕ bonds are increased and those for C_δ–N_ε and C_α–C_β bonds are decreased. In the case of N_ε–N_ϕ bond, the BCP electron density, ρ_3, is first increased and then decreased. At point P5 of the IRC profile, the corresponding BCP electron densities for C_β–C_δ and C_α–N_ϕ bonds reach to 0.23691 and 0.04840, respectively, while those for C_δ–N_ε and C_α–C_β bonds, respectively reach to 0.36131 and 0.26442. It is noteworthy that along the IRC profile of the reaction the BCP electron density corresponding to the C_β–C_δ bond, ρ_1, is more than that for C_α–N_ϕ one, ρ_4, thus it can be said that the former bond is formed faster than the later which is indicative of occurrence of an asynchronous concerted cycloaddition reaction between **NI** and **Aln** reagents. These results are consistent with those obtained from Fukui function analysis as well as Wiberg bond indexes.

Conclusion

Computational methods at B3LYP/6-311G** and wB97XD/6-311G** levels of theory were used to study the double 1,3-dipolar cycloaddition of nitrilimine with allenoate which was experimentally investigated by Guo and co-workers. For this purpose, four possible reactive channels were considered between nitrilimine and allenoates in both gas phase and dichloromethane solution which leads to the formation of four possible regioisomeric adducts. While regioselective generation of the experimentally reported adduct can clearly be explained using the analysis of calculated Fukui function reactivity indices, the Parr functions of the reactive sites of reactants fail to describe it accurately. Calculation and detection of transition states confirmed that the reactive channel which affords the experimentally reported adduct is kinetically the most favorable one. To study the charge transfer occurring in transition state, the global electron density transfer (GEDT) was calculated and the results indicated that all transition states are relatively polar. The Wiberg bond indexes and AIM analysis showed that all reactive channels take place via an asynchronous concerted mechanism, which is consistent with the Fukui functions analysis.

Methods

All calculations were performed using the Gaussian 09 program package [23]. For study of the cycloaddition reactions between **NI** and **Aln**, the structures of the reactants and products were optimized and their frequencies were calculated at B3LYP/6-311G** level of theory [24]. wB97XD/6-311G**

method was also used to consider the dispersion corrections for conformational analysis of **Aln** and optimization of the reactants, transition states, and products [25]. The conductor-like polarizable continuum model (CPCM) was used to calculate the solvation effects on the studied molecules in dichloromethane [26]. Transition states structures were determined using the Berny algorithm or the synchronous transit-guided quasi-Newton (STQN) procedure [27, 28]. The stationary points were characterized by frequency computations to verify that all transition states have one and only one imaginary frequency along the reaction coordinate. The structure of transition states was also confirmed using intrinsic reaction coordinates (IRC) calculations [29, 30].

The reactions rate constant k was calculated using Eyring equation:

$$k = \left(\frac{K_B T}{h}\right) exp\left(\frac{-\Delta G^{\ddagger}}{RT}\right)$$

where K_B is the Boltzmann constant, h is Plank's constant, T is the Kelvin temperature, $\Delta G^{\ddagger}$ is the free energy of activation and R is the universal gas constant [31]. The NBO analysis was performed to determine the atomic charges in the reactants, TS structures, and products [32, 33]. The nucleophilicity index N is defined as following equation in which, the HOMO energy of tetracyanoethylene (TCE), E_{HOMO}(Nu), is taken as the reference and E_{HOMO}(Nu) demonstrates the HOMO energy of nucleophile [34]:

$$N = E_{HOMO}(\text{Nu}) - E_{HOMO}(\text{TCE})$$

The electrophilicity index ω was calculated using the following equation [35]:

$$w = \frac{m^2}{2},$$

where μ and η represent the chemical potential and chemical hardness, respectively.

Acknowledgements I am thankful to the Research Council and Office of Graduate Studies of the University of Ayatollah Alozma Borujerdi for their financial support.

References

1. Huisgen R (1963) Angew Chem Int Ed 2:565
2. Hashimoto T, Maruoka K (2015) Chem Rev 115:5366
3. Bdiri B, Zhao B-J, Zhou Zh-M (2017) Tetrahedron Asymmetry 28:876
4. Moss GP (1999) Pure Appl Chem 71:531
5. Yavari I, Nematpour M, Sodagar E (2015) Monatsh Chem 146:2135
6. Abdou WM, Ganoub NA, Sabry E (2016) Monatsh Chem 147:619
7. Dawood KM (2005) J Heterocycl Chem 42:221
8. Monteiro Â, Gonçalves LM, Santos MMM (2014) Eur J Med Chem 79:266
9. Farghaly TA, Gomha SM, Dawood KM, Shaaban MR (2016) RSC Adv 6:17955
10. Dadiboyena S, Valente EJ, Hamme AT II (2014) Tetrahedron Lett 55:2208
11. Santos MMM (2014) Tetrahedron 70:9735
12. Liu H, Jia H, Wang B, Xiao Y, Guo H (2017) Org Lett 19:4714
13. Soleymani M, Dashti Khavidaki H (2017) Comp Theor Chem 1112:37
14. Memarian HR, Soleymani M, Sabzyan H (2012) J Iran Chem Soc 9:805
15. Memarian HR, Soleymani M, Sabzyan H, Bagherzadeh M, Ahmadi H (2011) J Phys Chem A 115:8264
16. Memarian HR, Sabzyan H, Soleymani M, Habibi MH, Suzuki T (2011) J Mol Struct 998:91
17. Geerlings P, De Proft F, Langenaeker W (2003) Chem Rev 103:1793
18. Yang W, Mortier WJ (1986) J Am Chem Soc 108:5708
19. Domingo LR, Pérez P, Sáez JA (2013) RSC Adv 3:1486
20. Chamorro E, Pérez P, Domingo LR (2013) Chem Phys Lett 582:141
21. Domingo LR (2014) RSC Adv 4:32415
22. Da Silva RR, Ramalho TC, Santos JM, Figueroa-Villar JD (2006) J Phys Chem A 110:1031
23. Frisch MJ, Trucks GW, Schlegel HB, Scuseria GE, Robb MA, Cheeseman JR, Scalmani G, Barone V, Mennucci B, Petersson GA, Nakatsuji H, Caricato M, Li X, Hratchia, HP, Izmaylov AF, Bloino J, Zheng G, Sonnenberg JL, Hada M, Ehara M, Toyota K, Fukuda R, Hasegawa J, Ishida M, Nakajima T, Honda Y, Kitao O, Nakai H, Vreven T, Montgomery JA, Peralta JE, Ogliaro F, Bearpark M, Heyd JJ, Brothers E, Kudin KN, Staroverov VN, Kobayashi R, Normand J, Raghavachari K, Rendell A, Burant JC, Iyengar SS, Tomasi J, Cossi M, Rega N, Millam JM, Klene M, Knox JE, Cross JB, Bakken V, Adamo C, Jaramillo J, Gomperts R, Stratmann RE, Yazyev O, Austin AJ, Cammi R, Pomelli C, Ochterski JW, Martin RL, Morokuma K, Zakrzewski VG, Voth GA, Salvador P, Dannenberg JJ, Dapprich S, Daniels A, Farkas O, Foresman JB, Ortiz JV, Cioslowski J, Fox DJ (2009) Gaussian 09, Revision E.01. Gaussian Inc, Wallingford, CT
24. Lee C, Yang W, Parr RG (1988) Phys Rev B 37:785
25. Chai JD, Head-Gordon M (2008) Phys Chem Chem Phys 10:6615
26. Barone V, Cossi M (1998) J Phys Chem A 102:1995
27. Schlegel HB (1982) J Comput Chem 3:214
28. Peng C, Ayala PY, Schlegel HB, Frisch MJ (1996) J Comput Chem 17:49
29. Gonzalez C, Schlegel HB (1989) J Chem Phys 90:2154
30. Gonzalez C, Schlegel HB (1990) J Phys Chem 94:5523
31. Eyring H (1935) J Chem Phys 3:107
32. Reed AE, Curtiss LA, Weinhold F (1988) Chem Rev 88:899
33. Carpenter JE, Weinhold F (1988) J Mol Struct 169:41
34. Domingo LR, Perez P, Ortega DE (2013) J Org Chem 78:2462
35. Parr RG, Szentpaly LV, Liu S (1999) J Am Chem Soc 121:1922